

# Variability of Nineteen Millisecond Pulsars in 47 Tucanae with *CHANDRA*/HRC-S

P. B. Cameron<sup>1</sup>, R. E. Rutledge<sup>2</sup>, F. Camilo<sup>3</sup>, L. Bildsten<sup>4</sup>, S. M. Ransom<sup>5</sup>, and  
S. R. Kulkarni<sup>1</sup>

## ABSTRACT

We present results from our 830 ksec observation of the globular cluster 47 Tucanae with the *Chandra X-ray Observatory's* High Resolution Camera-S. We limit our analysis here to the 19 previously known, localized millisecond pulsars (MSPs) in the cluster. This work more than doubles the sample of X-ray-detected MSPs observed with sensitivity to rotational variability; it is also the first survey of a large group of radio-discovered MSPs for which no previous X-ray pulsations have been detected and is therefore an unbiased survey of the X-ray properties of radio-discovered MSPs. We find that only 47 Tuc D, O and R show significant pulsations at the  $\gtrsim 4\text{-}\sigma$  level, but there is statistical evidence for rotational variability in five additional MSPs. Furthermore, we constrain the pulsed magnetospheric emission of 7 more MSPs using Monte Carlo simulations. The result is that the majority of the 47 Tuc MSPs are characterized by low pulsed fractions,  $\lesssim 50\%$ . In cases where larger pulsed fractions are measured the folded pulse profiles show relatively large duty cycles. When considered with previous spectroscopic studies, this suggests that the X-ray emission arises from the neutron star's heated polar caps, and in some cases, from intra-binary shocks, but generally not directly from the star's magnetosphere. We discuss the impact of these results on our understanding of high energy emission from MSPs.

---

<sup>1</sup>Division of Physics, Mathematics and Astronomy, California Institute of Technology, MS 105-24, Pasadena, CA 91125; pbc@astro.caltech.edu, srk@astro.caltech.edu

<sup>2</sup>Department of Physics, McGill University, Rutherford Physics Building, 3600 University Street, Montreal, QC H3A 2T8, Canada; rutledge@physics.mcgill.ca

<sup>3</sup>Columbia Astrophysics Laboratory, Columbia University, 550 West 120th Street, New York, NY 10027; fernando@astro.columbia.edu

<sup>4</sup>Kavli Institute for Theoretical Physics and Department of Physics, Kohn Hall, University of California, Santa Barbara, CA 93106; bildsten@kitp.ucsb.edu

<sup>5</sup>National Radio Astronomy Observatory, 520 Edgemont Road, Charlottesville, VA 22903; sransom@nrao.edu

*Subject headings:* globular clusters: individual (47 Tucanae) — pulsars: general  
 — stars: neutron — X-rays: stars

## 1. Introduction

Millisecond pulsars (MSPs) are old neutron stars spun-up by accretion of mass and angular momentum from the matter of a donor binary companion (Alpar et al. 1982). When compared to the canonical radio pulsar population they are distinguished by short spin periods,  $P \lesssim 25$  ms, small spin-down rates,  $\dot{P} \gtrsim 10^{-20}$  s/s, and thus low inferred dipole magnetic field strengths,  $B_{\text{dipole}} \propto (P\dot{P})^{1/2} \sim 10^{8-10}$  G, with large characteristic ages,  $\tau \equiv P/2\dot{P} \gtrsim 1$  Gyr. Studies of the  $\approx 150$  known MSPs are difficult at wavebands outside of the radio due to their intrinsic faintness. The vast majority ( $\approx 80\%$ ) of MSPs have binary companions that dominate at optical wavelengths, thus X-rays are an important avenue for studying MSPs.

Currently, only 16 MSPs outside of 47 Tucanae (NGC 104, hereafter 47 Tuc) have been detected in X-rays, and only 12 of these have been observed with sufficient time resolution to explore variability on rotational timescales (see Table 1). There are several proposed physical mechanisms capable of generating X-rays from these MSPs. Non-thermal emission processes in the neutron star magnetosphere generate power-law components in their X-ray spectra with characteristic photon indices  $\Gamma \approx 1.5-2$ . Pulsars in this class (e.g. PSRs B1937+21 and B1821–24A; those above the first horizontal line in Table 1) have large spin-down energies ( $\dot{E} \gtrsim 10^{35}$  erg s $^{-1}$ ), bright X-ray emission ( $L_X \gtrsim 10^{32}$  erg s $^{-1}$ ), low duty cycles and pulse profiles that closely resemble the radio emission in morphology and phase with large pulsed fractions,  $f_p \gtrsim 50\%$  (see §3.1). Power-law spectral components can also be produced when the wind from the MSP interacts with material from the binary companion causing an intra-binary shock. These pulsars have similar properties to those above, with the exception that they lack strong rotational modulation (e.g. the ‘black widow’ pulsar, PSR 1957+20). Finally, heating of the neutron star polar cap by the bombardment of relativistic particles provides a mechanism for producing thermal X-ray emission. MSPs dominated by thermal spectra (e.g. PSRs J0437–4715, J2124–3358; most of those below the first horizontal line in Table 1) are characterized by lower spin down energies ( $\dot{E} \lesssim 10^{34}$  erg s $^{-1}$ ), lower X-ray luminosities ( $L_X \lesssim 10^{32}$  erg s $^{-1}$ ) and pulse profiles with large duty cycles. As seen in Table 1, the pulsed fractions of these MSPs are usually poorly constrained, but generally show  $f_p \approx 50\%$ . The emission of thermal cooling X-rays from the neutron star surface and those from pulsar wind nebulae are not thought to be important for these old objects, so we will not consider them here.

The unprecedented spatial resolution of *Chandra* has enabled detailed studies of MSPs in globular clusters. Observations of M28, M4, NGC 6397, M30 and others have provided the first census of low-luminosity X-ray sources in these clusters (Rutledge et al. 2004; Becker et al. 2003; Bassa et al. 2004; Grindlay et al. 2002; Ransom et al. 2004). However, the largest endeavor has been *Chandra*'s observing campaign of 47 Tuc (Grindlay et al. 2001, 2002; Heinke et al. 2005; Bogdanov et al. 2006). This work has shown that the spectral characteristics of the 47 Tuc MSPs are relatively homogeneous. Their luminosities fall in a narrow range,  $L_X \approx 10^{30-31}$  erg s $^{-1}$ , and are well described by thermal spectral models with small emission radii,  $R_{\text{eff}} \approx 0.1\text{-}3$  km and temperatures of  $T_{\text{eff}} \approx 1\text{-}3 \times 10^6$  K. The only exceptions are the radio-eclipsing binaries 47 Tuc J, O and W, which require additional power-law components above 2 keV with  $\Gamma \approx 1.0\text{-}1.5$ . These results are reinforced by the findings of detailed spectroscopic studies by *Chandra* and *XMM-Newton* that have emphasized the dominant thermal components in nearby MSP X-ray spectra over the fainter power-law features (Zavlin et al. 2002; Zavlin 2006). Consequently, we expect the predominant X-ray emission from the MSPs in 47 Tuc to arise from heated polar caps, and to be modulated just by rotating a small area relative to the observer (i.e. sinusoidal pulse profiles; Grindlay et al. 2002; Cheng & Taam 2003; Bogdanov et al. 2006).

In this paper, we present high time resolution data capable of exploring the fast time variability of the X-ray counterparts to the 47 Tuc MSPs. In § 2 we present the details of the observations and data reduction, followed by the variability analysis (§ 3) and an examination of the accuracy of the HRC-S time tags (§ 4). We find that the HRC-S remains capable of detecting fast modulation, but the MSPs in 47 Tuc lack strong variability on all timescales probed. We discuss the impact of this result on our understanding of the X-ray emission from MSPs in § 5.

## 2. Observations and Data Reduction

Observations of 47 Tuc were performed with *Chandra*'s HRC-S detector (Zombeck et al. 1995; Murray et al. 1998). They began 2005 Dec 19 7:20 UT with 14 subsequent visits over the next 20 days for a total of 833.9 ks of exposure time (see Table 2 for a summary). The observing plan of dividing the 833.9 ksec into 50–100 ksec visits spread out over 20 days was adopted – instead of the optimal choice for pulsar detection of an uninterrupted observation – to mitigate a thermal limitation in space-craft operations. The HRC-S has a timing resolution of 15.625  $\mu$ s in the nominal energy range of 0.1–2 keV, although it has essentially no energy

resolution. The data were analyzed using Chandra Interactive Analysis of Observations<sup>1</sup> software (CIAO) version 3.3 and CALDB version 3.2.1.

We began the data analysis of each observation by registering it to the first pointing (ObsID 5542) using the relative astrometry of the four brightest sources in the field. These corrections typically resulted in  $\lesssim 0''.5$  corrections to the native astrometry. Data were filtered on pulse invariant (PI) channel to maximize the signal-to-noise ratio (SNR) for the known MSPs using the following approach. We compared the PI channel distribution of all counts extracted from regions corresponding to the known MSPs with that extracted from a background region. The background and source PI distributions are identical below  $\text{PI} = 25$  (within 1% in counts/area). Above this value the source region counts are significantly in excess, so we adopt  $\text{PI} = 25$  as the lower PI limit for background filtering. We determined the upper-limit in PI channel by maximizing the total source SNR, finding the maximum when data at  $\text{PI} > 120$  are excluded from analysis. Thus, we adopt a PI range of 25–120 for all analyses; this decreases the MSP source count rates by 6%, while excluding 51% of the total background counts. The resulting background contribution is 17.9 counts arcsec<sup>-2</sup> over the entire observing span.

Currently, positions are known for 19 of the 22 MSPs in 47 Tuc. Published pulsar timing solutions can account for 16 of these positions (Freire et al. 2001, 2003), while 47 Tuc R and Y have unpublished solutions (Freire et al. in preparation). 47 Tuc W has only a preliminary timing solution, but was localized by the eclipses of its optical counterpart (Freire et al. unpublished; Edmonds et al. 2002). The close proximity of pulsars 47 Tuc G and I and 47 Tuc F and S (separations  $0''.12$  and  $0''.7$ , respectively) do not allow them to be resolved by *Chandra*, so their counts must be considered jointly. For analysis purposes we attribute 50% of detected photons to each pulsar (see §3.1).

We extracted photons from within circular regions surrounding each of the known MSP positions. The size of each extraction region can be found in Table 3. The radius was chosen adaptively in order to maximize SNR, but constrained to mitigate contamination by nearby objects. However, some contamination due to source crowding is unavoidable. We estimate this contribution by modeling the PSF as a Gaussian with  $\sigma = 0.29''$ , calculating the number of photons that fall in the extraction region of a given source from each neighboring source, and using this estimate to update the extracted source counts. We iterate this procedure until we have an estimate of the source crowding contamination for all sources in the field. This analysis shows that the contamination is negligible ( $< 1\%$  of extracted counts) for all MSPs except O and R, which each have  $\sim 13$  additional background counts due to

---

<sup>1</sup><http://cxc.harvard.edu/ciao/>

nearby sources. We include these in our estimate of their backgrounds in the subsequent analysis (Table 3). Assuming these background estimates, we detect sources at each of the 17 independent pulsar positions with  $> 5\text{-}\sigma$  significance.

Throughout the analysis we assume a distance of 4.85 kpc to 47 Tuc (Gratton et al. 2003). We apply an energy correction factor of  $5.044 \times 10^{-12} \text{ erg cm}^{-2} \text{ s}^{-1}$  or  $1.42 \times 10^{34} \text{ erg s}^{-1}$  (0.5–2.0 keV) per 1 HRC-S count/sec, which is the unabsorbed X-ray flux assuming  $N_{\text{H}} = 1.3 \times 10^{20} \text{ cm}^{-2}$  and blackbody emission with a temperature of 0.178 keV determined from WebPIMMS<sup>2</sup> (Bogdanov et al. 2006). In addition to the extraction region size, we list the total counts extracted, expected background counts and the time averaged luminosity in Table 3.

### 3. Variability Analysis

Prior to the timing analysis, we use the CIAO tool `axbary` to convert the event times to the solar system barycenter using the JPL DE200 solar system ephemeris, the *Chandra* orbital ephemeris and the radio/optical position of each MSP (see § 2).

#### 3.1. Rotational Variability

We calculated the rotational phase of each arriving photon for each MSP using the latest radio ephemerides corrected to X-ray frequencies (Freire et al. 2003; Freire et al., in preparation). The resulting phases were searched for variability with the  $Z_n^2$ -test (Buccheri et al. 1983), where  $n$  is the optimal number of harmonics as determined from the H-test (de Jager et al. 1989). The variable  $Z_n^2$  has a probability density function distributed as  $\chi^2$  with  $2n$  degrees of freedom. We list the value of this variable, the detection significance in equivalent Gaussian  $\sigma$  and  $n$  in Table 3. Only 47 Tuc D, O and R show variability above the  $\approx 4\text{-}\sigma$  level. Their folded pulse profiles are shown in Figure 1. All three pulsars’ profiles are characterized by large duty cycles. 47 Tuc O shows evidence for two peaks centered at phases,  $\phi \approx 0.0$  and  $\phi \approx 0.4$  with widths of  $\delta\phi \approx 0.2$  and  $\delta\phi \approx 0.4$ , respectively. Only a single peak is evident in the profiles of 47 Tuc D and R centered at  $\phi \approx 0.45$  with  $\delta\phi \approx 0.25$  and  $\phi \approx 0.5$  with  $\delta\phi \approx 0.3$ , respectively.

As seen in Table 3, 5 of the 19 MSPs are detected with marginal significance, 2.8–3.3- $\sigma$ . Given the relatively large size of our MSP sample, we can quantify the significance of these marginal detections. We are free to choose the significance level with which we call an

---

<sup>2</sup><http://heasarc.gsfc.nasa.gov/Tools/w3pimms.html>

MSP ‘variable’. Once we choose this level, the problem becomes one of binomial statistics where each MSP represents an independent measurement for variability. Choosing the 99% percent confidence level for  $Z_n^2$  (corresponding to  $2.58\text{-}\sigma$ ) allows us to identify 8 ‘variable’ sources when only  $\approx 0.2$  are expected if the MSPs were drawn from a random distribution. The probability of 8 of 19 trials being labeled ‘variable’ is  $6.7 \times 10^{-12}$ . The probability of one or more of these being false detections is 17.4%. Since the confidence level at which we label an MSP as ‘variable’ is arbitrary, we list a range of confidence levels and the number of corresponding detections with the binomial and false detection probabilities in Table 4. For the remainder of our analysis we will adopt the 99% confidence level. This results in 47 Tuc D, E, F, H, O, Q, R and S being labeled as ‘variable.’ Their profiles are shown in Figure 1.

The pulsed fraction,  $f_p$ , for each MSP can be determined using two steps. First, we estimate the DC (unpulsed) level with the non-parametric bootstrapping method of Swanepoel et al. (1996). The advantage of this technique is that it works on the raw phases without the need to construct a phase histogram or know the pulse shape a priori. This level is shown by the solid line in Figure 1 with  $\pm 1\text{-}\sigma$  errors. Next, we correct for the fact that the DC component includes both unpulsed photons from the MSP and background photons. Note that for MSPs F and S we consider 50% of the background subtracted source counts to be unpulsed background photons. The expected background contribution to the pulse profile is denoted by the dashed line in Figure 1 (see § 2). The pulsed fraction determined by the bootstrapping method can be related to the true pulsed fraction by  $f_p = f_{p,\text{boot}} N_t / (N_t - N_b)$ , where  $f_{p,\text{boot}}$  is the pulsed fraction determined by the bootstrapping method,  $N_t$  is the total number of extracted counts and  $N_b$  is the total number of background counts contributing to  $N_t$ . Both  $N_t$  and  $N_b$  can be found in Table 3. The pulsed fractions derived in this manner are also listed in Table 3.

We calculate upper limits on the pulsed fractions of the remaining 11 MSPs with timing solutions (note that W has only a preliminary solution) with Monte Carlo simulations assuming two scenarios. First, we make the conservative assumption that the underlying pulse shape is sinusoidal. For each MSP and pulsed fraction we simulate 500 light curves with a total number of counts  $N_t = N_b + N_s$ , where  $N_s$  is the number of source counts. If the pulsed fraction is  $f_{p,\text{sine}}$ , then  $N_s$  consists of  $(1 - f_{p,\text{sine}})N_s$  unpulsed counts and  $f_{p,\text{sine}}N_s$  pulsed counts. For the two unresolved MSPs that do not show pulsations (G and I) we assume that 50% of the source photons constitute an unpulsed background. We determine the 90% confidence upper limit on the pulsed fraction as the value of  $f_{p,\text{sine}}$  at which 450 synthetic light curves have values of  $Z_1^2 \gtrsim 27.4$  (corresponding to  $5\text{-}\sigma$ ). The result is that only J, L, W and Y have sufficient counts to be constrained in this way.

Motivated by the close correspondence of the radio and X-ray pulse profiles of magnetospherically dominated MSPs (see § 1), we determine a second set of upper limits based on the assumption that the underlying X-ray pulse has the same morphology as the radio pulse. We denote this pulsed fraction as  $f_{p,\text{radio}}$ . In the case of the weak radio pulsars, N, R, T, W and Y it was necessary to model the radio pulse(s) with Gaussians and use these as the assumed X-ray pulse shape. The radio pulse profiles for remaining MSPs have sufficient signal-to-noise to be used directly. We then perform the Monte Carlo simulations with the technique described above to determine the 90% confidence upper limits. The results can be found in Table 3. It is possible to constrain the X-ray emission with the same morphology as the radio pulse from 7 pulsars in this way.

### 3.2. Orbital Variability

The orbital periods of the 12 binary 47 Tuc MSPs span the range 0.07–2.4 days. In order to search for variability during these orbits we calculated the orbital phase of each arriving photon for each MSP and constructed histograms with 5, 10 and 20 bins. We then corrected each bin for the variation of exposure time during that particular orbital phase so that we have a histogram of counts per second per bin and subtracted the expected background contribution. We search for variability by computing  $\chi^2$  between the histogram and a constant count rate. We found that none of the 47 Tuc binary MSPs showed significant orbital variability.

Substantial X-ray eclipses characterized by a complete disappearance of hard ( $> 2$  keV) photons and a decline in soft ( $< 2$  keV) photons for  $\approx 30\%$  of the orbit have been reported for 47 Tuc W (Bogdanov et al. 2005). Thus, the lack orbital variability in 47 Tuc W is surprising. We reduced archival ACIS-S data of 47 Tuc W from ObsIDs 2735, 2736, 2737, and 2739 in order to quantify the properties of the eclipse in the HRC-S bandpass. We reprocessed the level 1 event files to make use of the latest calibration and filtered periods of high background flaring (i.e. periods with count rates  $> 3\sigma$  above the mean full-frame rate). This resulted in 251.3 ksec of exposure time. We computed the orbital phase of each photon within a  $1''$  radius of the position of 47 Tuc W in the energy range 0.3–2.0 keV with the preliminary timing solution (see § 2). The X-ray eclipse is evident in the histogram shown in Figure 2a at phase,  $\phi \approx 0.2$ , where  $\phi = 0$  at the time of the ascending node. This X-ray eclipse timing agrees well with observed radio eclipse from  $\phi = 0.1$ –0.4 (Camilo et al. 2000; Edmonds et al. 2002). The variability is significant at the  $4.3\sigma$  level from the measured value of  $Z_1^2 = 30.1$  and we determine an orbital modulation of  $f_p = 36 \pm 9\%$  using the non-parametric bootstrap method (see § 3.1). This is consistent with the 90% confidence

limit of  $f_{p,\text{ sine}} < 48\%$  on a sinusoidal signal in the HRC-S time series of 47 Tuc W (see § 3.1).

### 3.3. Aperiodic Variability

To search for aperiodic variability in the 47 Tuc MSPs, we have applied the Bayesian blocks algorithm of Scargle (1998) as implemented by the Interactive Spectral Interpretation System (ISIS; Houck & Denicola 2000). The algorithm determines the optimal decomposition of the light curve into constant count rate segments based on a parametric maximum likelihood model of a Poisson process. The raw (unbinned) events are divided into ‘blocks’ and the odds ratio that the count rate has varied is computed. If variability is found, each ‘block’ is further subdivided to characterize the structure of the light curve (e.g. step-function variation, flaring, etc.). We could not identify any intra-observation variability from 17 MSPs using an odds ratio corresponding to 68% chance that any variability is real. In addition, the inter-observation count rates for each MSP derived from this process do not show significant variability over the  $\approx 20$  day span of our observations. Thus, the X-ray emission from the 47 Tuc MSPs is stable on timescales ranging from minutes to days.

### 3.4. ACIS-S vs. HRC-S Comparison

With such a large sample of constant luminosity X-ray sources, we can compare the count rates between the ACIS-S and HRC-S for soft thermal sources. In Figure 3 we compare the count rate for the two detectors using each of the 17 independent MSP detections. For the ACIS-S count rate, we summed the values in the 0.3–0.8 keV and 0.8–2.0 keV bands listed by Heinke et al. (2005). The relation between count rates in the two different detectors was  $I(\text{HRC} - \text{S}) = (0.43 \pm 0.024) \times I(\text{ACIS} - \text{S})$ . This is consistent with the conversion from HRC-S to ACIS-I (Rutledge et al. 2004).

## 4. HRC-S Timing Accuracy

The accuracy of the HRC-S time tags was demonstrated to be  $\pm 12 \mu\text{s}$  in an observation of M28 (Rutledge et al. 2004). We have investigated several issues to ensure that the HRC-S has sufficient accuracy to detect MSPs. In addition to accounting for a leap second that occurred during the middle of the observing span, we examined the effect of telemetry saturation, different solar system ephemerides and analyzed a recent calibration observation of the globular cluster M28.



#### 4.1. Telemetry Saturation

The maximum telemetered full-field, unfiltered count rate for the HRC-S is 184 counts  $s^{-1}$  (*Chandra* Proposers’ Observatory Guide <sup>3</sup>). At rates above this, a decreasing fraction of all counts will be telemetered. The data will be affected if this count rate is exceeded during the 2.05 s full-frame readout time. The effect of telemetry saturation on timing certainty is that, when telemetry is saturated, not all events are telemetered back to Earth. Due to the HRC wiring error (Tennant et al. 2001), the  $N$ th event detected by the HRC-S has its time assigned to the  $N+1$ st event<sup>8</sup>. The true time series can be reconstructed if both are telemetered; if either is not, then the wrong time will be assigned to one event (either the  $N$ th event, or the  $N - 1$ st event).

To test the extent to which this saturation impacts our observations we constructed a light curve of our entire dataset binned in 2.05 s intervals. We found that only  $\approx 0.1\%$  of the bins exceeded the maximum count rate. Thus telemetry saturation will effect only  $\approx 0.1\%$  of the counts in any given MSP, which is negligible.

#### 4.2. Ephemeris Comparison

We performed a preliminary extraction of data using DE405 and compared the timing precision of data corrected to DE200 using one of the brightest sources in the field. We found the entire observational period was offset by  $t_{DE405} - t_{DE200} = 1.3809$  ms at the start of the observational period, decreasing monotonically to 1.3719 ms at the end of the observation period. Thus, there was an average direct offset between the photon time-of-arrivals (TOAs) in the two ephemerides of  $\approx 1.3764$  ms, and a range of variation of  $\approx 9 \mu s$ . This  $9 \mu s$  therefore amounts to the relative timing uncertainty due to the adopted ephemeris, comparable to the uncertainties in HRC digitization ( $\pm 5 \mu s$ ) and *Chandra* clock stability ( $\pm 5 \mu s$ ) (Rutledge et al. 2004).

#### 4.3. s/c Clock Stability

A calibration observation of PSR B1821–24A was performed on May 27, 2006 starting at 12:30 UT for 40887 sec in order to evaluate the stability of the HRC-S clock. A complete analysis is beyond the scope of this work. However, a search of the data using the known radio

---

<sup>3</sup><http://cxc.harvard.edu/proposer/POG/index.html>

timing ephemeris (Rutledge et al. 2004) clearly detects the 3.05 ms pulsar with  $Z_1^2 = 330$  corresponding to a detection significance of  $\approx 18\text{-}\sigma$ . Thus, we conclude the HRC-S clock has remained sufficiently stable to detect MSPs.

## 5. Discussion and Conclusions

*Chandra* HRC-S observations of 47 Tuc have allowed us to study a relatively large sample of 19 MSPs on millisecond to week timescales. We find that the MSPs in 47 Tuc uniformly show very low levels of variability on all scales probed. We have sufficient statistics to meaningfully constrain (under the assumption that their X-ray pulse profiles match the radio) or measure the rotational modulation of 15 MSPs. Eight of these objects have low pulsed fractions,  $f_p \lesssim 50\%$ . MSPs 47 Tuc D, O, and R each have pulsations detected at  $\gtrsim 4\text{-}\sigma$  significance with relatively large pulsed fractions,  $f_p \gtrsim 60\%$ , which are similar to the levels seen from luminous MSPs dominated by non-thermal emission (e.g. PSRs B1821–24A and B1937+21). However, the pulse profiles of these objects (see Figure 1) are characterized by large duty-cycle features that do not resemble the sharp, low duty-cycle profiles seen in the non-thermal MSPs (e.g. see Becker & Aschenbach 2002).

The existing ACIS data show that the 47 Tuc MSPs have fairly homogeneous spectroscopic properties (Grindlay et al. 2002; Bogdanov et al. 2006). All but 3 of the 47 Tuc MSPs are characterized by  $1\text{--}3 \times 10^6$  K thermal spectra with low luminosities in a narrow range,  $L_X \approx 10^{30\text{--}31}$  erg s $^{-1}$ , and have small emission radii,  $R_{\text{eff}} \approx 0.1\text{--}3.0$  km. The low level of measured variability presented here indicates that rotational averaging does little to affect these values, which agree with the predictions of polar cap heating scenarios (Harding & Muslimov 2002). Thus we conclude that, unlike the luminous non-thermal MSPs, the vast majority of the X-ray emission from the 47 Tuc MSPs is created by the heating of the neutron star polar cap by a return current of relativistic particles produced in the magnetosphere (Arons 1981; Harding & Muslimov 2001, 2002; Grindlay et al. 2002; Bogdanov et al. 2006). For older MSPs with very short spin periods and low magnetic fields, like those in 47 Tuc, the main source of the  $e^\pm$ -pair production is thought to be through inverse Compton scattering of thermal X-rays from the neutron star surface off of electrons in the pulsar magnetosphere (Harding & Muslimov 2002).

Only the radio-eclipsing binaries 47 Tuc J, O and W show power-law spectral components that contribute significantly (70%, 50% and 75%, respectively) to their total flux (Bogdanov et al. 2006). The lack of strongly pulsed emission in 47 Tuc J and W suggests that the X-ray emission does not arise in the neutron star magnetosphere, but instead is likely the consequence of an intra-binary shock. This is in agreement with conclusions based

on orbital phase resolved spectroscopy of 47 Tuc W by Bogdanov et al. (2005). Conversely, the current data do not conclusively identify the origin of X-rays from 47 Tuc O, which shows significant pulsations. The X-rays from an intra-binary shock are not expected to be modulated at the rotational period of the MSP, so the measured pulsed fraction,  $f_p = 83 \pm 21\%$ , is only marginally consistent with the 50% spectroscopic allocation of X-rays due to a shock. In addition, its large duty-cycle does not immediately imply that polar cap heating is the source of the pulsed X-rays, since broadly beamed magnetospheric emission viewed off-axis would appear to have a large duty-cycle (Becker & Trümper 1999).

The apparent non-detection of low duty-cycle pulsars is significant in comparison with the pulse profile of B1821–24A. If all 19 MSPs had X-ray pulse profiles identical to that of PSR B1821–24A, all would have been detected with  $\gtrsim 7\text{-}\sigma$  significance (which we find for the lowest SNR MSP, 47 Tuc T). Those MSPs with higher count rates would have been detected with even greater significance. The implication is that PSR B1821–24A has an unusually low duty cycle for a MSP. If we assume that low duty-cycle MSPs make up a fraction  $f$  of the globular cluster population, then the non-detection of even 1 such pulsar in 47 Tuc implies that B1821–24A-like pulsars comprise  $f < 20\%$  of the MSP population in GCs (90% confidence limit). This limit could be much lower, if the intrinsic distribution of duty cycles in magnetospheric pulsars is lower than that of B1821–24A, for example; however, there seems to be little observational work quantifying the distribution of duty cycles of observed pulsars.

The authors would like to thank P. Freire for providing us with data prior to publication. Support for this work was provided by NASA through Chandra Award Number G05-6060 issued by the Chandra X-ray Observatory Center, which is operated by the Smithsonian Astrophysical Observatory for and on behalf of NASA under contract NAS8-03060. L. B. acknowledges support from the NSF through grant PHY99-07949.

*Facilities:* CXO (HRC)

## REFERENCES

- Alpar, M. A., Cheng, A. F., Ruderman, M. A., & Shaham, J. 1982, *Nature*, 300, 728
- Arons, J. 1981, *ApJ*, 248, 1099
- Bassa, C., Pooley, D., Homer, L., Verbunt, F., Gaensler, B. M., Lewin, W. H. G., Anderson, S. F., Margon, B., Kaspi, V. M., & van der Klis, M. 2004, *ApJ*, 609, 755

- Becker, W., & Trümper, J. 1999, *A&A*, 341, 803
- Becker, W. & Aschenbach, B. 2002, in *Neutron Stars, Pulsars, and Supernova Remnants*, ed. W. Becker, H. Lesch, and J. Trümper (MPE Rep. 278; Carching: MPE), 64
- Becker, W., Swartz, D. A., Pavlov, G. G., Elsner, R. F., Grindlay, J., Mignani, R., Tennant, A. F., Backer, D., Pulone, L., Testa, V., & Weisskopf, M. C. 2003, *ApJ*, 594, 798
- Becker, W. & Trümper, J. 1999, *A&A*, 341, 803
- Blandford, R., & Teukolsky, S. A. 1976, *ApJ*, 205, 580
- Bogdanov, S., Grindlay, J. E., Heinke, C. O., Camilo, F., Freire, P. C. C., & Becker, W. 2006, *ApJ*, 646, 1104
- Bogdanov, S., Grindlay, J. E., & van den Berg, M. 2005, *ApJ*, 630, 1029
- Buccheri, R., Bennett, K., Bignami, G. F., Bloemen, J. B. G. M., Boriakoff, V., Caraveo, P. A., Hermsen, W., Kanbach, G., Manchester, R. N., Masnou, J. L., Mayer-Hasselwander, H. A., Ozel, M. E., Paul, J. A., Sacco, B., Scarsi, L., & Strong, A. W. 1983, *A&A*, 128, 245
- Camilo, F., Lorimer, D. R., Freire, P., Lyne, A. G., & Manchester, R. N. 2000, *ApJ*, 535, 975
- Cheng, K. S. & Taam, R. E. 2003, *ApJ*, 598, 1207
- Cordes, J. M. & Lazio, T. J. W. 2002, preprint (astro-ph/0207156)
- D’Amico, N., Possenti, A., Fici, L., Manchester, R. N., Lyne, A. G., Camilo, F., & Sarkissian, J. 2002, *ApJ*, 570, L89
- D’Amico, N., Possenti, A., Manchester, R. N., Sarkissian, J., Lyne, A. G., & Camilo, F. 2001, *ApJ*, 561, L89
- de Jager, O. C., Raubenheimer, B. C., & Swanepoel, J. W. H. 1989, *A&A*, 221, 180
- Edmonds, P. D., Gilliland, R. L., Camilo, F., Heinke, C. O., & Grindlay, J. E. 2002, *ApJ*, 579, 741
- Freire, P. C., Camilo, F., Kramer, M., Lorimer, D. R., Lyne, A. G., Manchester, R. N., & D’Amico, N. 2003, *MNRAS*, 340, 1359
- Freire, P. C., Camilo, F., Lorimer, D. R., Lyne, A. G., Manchester, R. N., & D’Amico, N. 2001, *MNRAS*, 326, 901

- Gratton, R. G., Bragaglia, A., Carretta, E., Clementini, G., Desidera, S., Grundahl, F., & Lucatello, S. 2003, *A&A*, 408, 529
- Grindlay, J. E., Camilo, F., Heinke, C. O., Edmonds, P. D., Cohn, H., & Lugger, P. 2002, *ApJ*, 581, 470
- Grindlay, J. E., Heinke, C., Edmonds, P. D., & Murray, S. S. 2001, *Science*, 292, 2290
- Harding, A. K. & Muslimov, A. G. 2001, *ApJ*, 556, 987
- . 2002, *ApJ*, 568, 862
- Heinke, C. O., Grindlay, J. E., Edmonds, P. D., Cohn, H. N., Lugger, P. M., Camilo, F., Bogdanov, S., & Freire, P. C. 2005, *ApJ*, 625, 796
- Houck, J. C. & Denicola, L. A. 2000, in *ASP Conf. Ser. 216: Astronomical Data Analysis Software and Systems IX*, ed. N. Manset, C. Veillet, & D. Crabtree, 591
- Lange, C., Camilo, F., Wex, N., Kramer, M., Backer, D. C., Lyne, A. G., & Doroshenko, O. 2001, *MNRAS*, 326, 274
- Lommen, A. N., Zepka, A., Backer, D. C., McLaughlin, M., Cordes, J. M., Arzoumanian, Z., & Xilouris, K. 2000, *ApJ*, 545, 1007
- Murray, S. S., Chappell, J. H., Kenter, A. T., Kraft, R. P., Meehan, G. R., & Zombeck, M. V. 1998, in *Proc. SPIE Vol. 3356, Space Telescopes and Instruments V*, Pierre Y. Bely; James B. Breckinridge; Eds., 974
- Navarro, J., de Bruyn, A. G., Frail, D. A., Kulkarni, S. R., & Lyne, A. G. 1995, *ApJ*, 455, L55
- Nicastro, L., Cusumano, G., Löhmer, O., Kramer, M., Kuiper, L., Hermsen, W., Mineo, T., & Becker, W. 2004, *A&A*, 413, 1065
- Nice, D. J., Splaver, E. M., Stairs, I. H., Löhmer, O., Jessner, A., Kramer, M., & Cordes, J. M. 2005, *ApJ*, 634, 1242
- Ransom, S. M., Stairs, I. H., Backer, D. C., Greenhill, L. J., Bassa, C. G., Hessels, J. W. T., & Kaspi, V. M. 2004, *ApJ*, 604, 328
- Rutledge, R. E., Fox, D. W., Kulkarni, S. R., Jacoby, B. A., Cognard, I., Backer, D. C., & Murray, S. S. 2004, *ApJ*, 613, 522
- Scargle, J. D. 1998, *ApJ*, 504, 405

- Swanepoel, J. W. H., de Beer, C. F., & Loots, H. 1996, *ApJ*, 467, 261
- Takahashi, M., Shibata, S., Torii, K., Saito, Y., Kawai, N., Hirayama, M., Dotani, T., Gunji, S., Sakurai, H., Stairs, I. H., & Manchester, R. N. 2001, *ApJ*, 554, 316
- Tennant, A. F., Becker, W., Juda, M., Elsner, R. F., Kolodziejczak, J. J., Murray, S. S., O’Dell, S. L., Paerels, F., Swartz, D. A., Shibasaki, N., & Weisskopf, M. C. 2001, *ApJ*, 554, L173
- Thorsett, S. E., Arzoumanian, Z., Camilo, F., & Lyne, A. G. 1999, *ApJ*, 523, 763
- Toscano, M., Sandhu, J. S., Bailes, M., Manchester, R. N., Britton, M. C., Kulkarni, S. R., Anderson, S. B., & Stappers, B. W. 1999, *MNRAS*, 307, 925
- Webb, N. A., Olive, J.-F., & Barret, D. 2004a, *A&A*, 417, 181
- Webb, N. A., Olive, J.-F., Barret, D., Kramer, M., Cognard, I., & Löhmer, O. 2004b, *A&A*, 419, 269
- Zavlin, V. E. 2006, *ApJ*, 638, 951
- Zavlin, V. E., Pavlov, G. G., Sanwal, D., Manchester, R. N., Trümper, J., Halpern, J. P., & Becker, W. 2002, *ApJ*, 569, 894
- Zombeck, M. V., Chappell, J. H., Kenter, A. T., Moore, R. W., Murray, S. S., Fraser, G. W., & Serio, S. 1995, in *Proc. SPIE Vol. 2518, EUV, X-Ray, and Gamma-Ray Instrumentation for Astronomy VI*, Oswald H. Siegmund; John V. Vallerger; Eds., 96

Table 1. X-ray Properties of Millisecond Pulsars Outside of 47 Tuc.

| PSR                             | $P$<br>(ms) | $d$<br>(kpc)      | $\tau$<br>(Gyr) | $\log \dot{E}$<br>(erg s <sup>-1</sup> ) | $\log L_X$<br>(erg s <sup>-1</sup> ) | $f_p$<br>(%)         | Refs. |
|---------------------------------|-------------|-------------------|-----------------|--|--------------------------------------|----------------------|-------|
| B1937+21                        | 1.56        | 3.57              | 0.23            | 36.04                                    | 33.15                                | 54 ± 7               | 1,2   |
| B1957+20                        | 1.61        | 2.49              | 2.22            | 35.04                                    | 31.81                                | < 60                 | 1,3   |
| J0218+4232                      | 2.32        | 2.67              | 0.48            | 35.38                                    | 32.54                                | 59 ± 7               | 4,5   |
| B1821–24A (M28)                 | 3.05        | 5.5 <sup>a</sup>  | 0.03            | 36.35                                    | 33.22                                | 85 ± 3               | 6,7   |
| J0751+1807                      | 3.48        | 1.15              | 7.08            | 33.86                                    | 30.84                                | 52 ± 8 <sup>b</sup>  | 8,9   |
| J0030+0451                      | 4.87        | 0.32              | 7.71            | 33.53                                    | 30.40                                | 69 ± 18              | 10,11 |
| J2124–3358                      | 4.93        | 0.25              | 6.01            | 33.83                                    | 30.23                                | 56 ± 14              | 1,12  |
| J1012+5307                      | 5.26        | 0.84              | 4.86            | 33.68                                    | 30.38                                | 77 ± 13 <sup>b</sup> | 13,9  |
| J0437–4715                      | 5.76        | 0.14 <sup>a</sup> | 4.91            | 33.58                                    | 30.47                                | 40 ± 2               | 14,12 |
| J1024–0719                      | 5.16        | 0.39              | 27              | 32.93                                    | 29.30                                | 52 ± 22              | 1,12  |
| J1744–1134                      | 4.07        | 0.36 <sup>a</sup> | 9.1             | 33.62                                    | 29.49 <sup>c</sup>                   | —                    | 1,3   |
| J0034–0534                      | 1.88        | 0.54              | 6.03            | 34.48                                    | 29.60 <sup>c</sup>                   | —                    | 12    |
| No High Time Resolution Imaging |             |                   |                 |  |                                      |                      |       |
| B1620–26 (M4)                   | 11.08       | 1.73 <sup>a</sup> | 0.26            | 34.28                                    | 30.08 <sup>c</sup>                   | —                    | 15,16 |
| J1740–5340 (NGC 6397)           | 3.65        | 2.55 <sup>a</sup> | 0.34            | 35.15                                    | 30.9 <sup>c</sup>                    | —                    | 17,18 |
| J1911–6000C (NGC 6752)          | 5.28        | 4.1 <sup>a</sup>  | 38.1            | 32.77                                    | 30.34 <sup>c</sup>                   | —                    | 19    |
| J2140–2310A (M30)               | 11.02       | 9.0 <sup>a</sup>  | >0.08           | <34.79                                   | 30.64 <sup>c</sup>                   | —                    | 20    |

<sup>a</sup>Accurate distance measurement.

<sup>b</sup>Detection significance is low.

<sup>c</sup>X-ray luminosity in the 0.5–2.5 keV band.

Note. — All distances are estimated from the pulsar dispersion measures and the model of Galactic distribution of free electrons (Cordes & Lazio 2002), except where noted. X-ray luminosities are quoted in the 0.2–10 keV band as adopted from Table 1 of Zavlin (2006) and references therein, except where noted. Pulsed fractions are quoted in roughly in the HRC-S band (0.1–2.0 keV), but see references for the specific bandpass. The spectra of MSPs above the first horizontal line are dominated by non-thermal X-ray emission. Those below the line have significant thermal components or are indeterminate (and thus presumed to be thermal) in nature. References: 1 – Toscano et al. (1999), 2 – Nicastro et al. (2004), 3 – Becker & Trümper (1999), 4 – Navarro et al. (1995), 5 – Webb et al. (2004a), 6 – Becker et al. (2003), 7 – Rutledge et al. (2004), 8 – Nice et al. (2005), 9 – Webb et al. (2004b), 10 – Lommen et al. (2000), 11 – Becker & Aschenbach (2002), 12 – Zavlin (2006) 13 – Lange et al. (2001), 14 – Zavlin et al. (2002), 15 – Thorsett et al. (1999), 16 – Bassa et al. (2004), 17 – D’Amico et al. (2001), 18 – Grindlay et al. (2002), 19 – D’Amico et al. (2002), 20 – Ransom et al. (2004).

Table 2. HRC-S Observations.

| ObsID | Obs. Start<br>(UT) | Obs. Start<br>(MJD) | Exp. Time<br>(sec) |
|-------|--------------------|---------------------|--------------------|
| 5542  | 2005 Dec 19.29     | 53723.79            | 51918.2            |
| 5543  | 2005 Dec 20.62     | 53725.12            | 53962.6            |
| 5544  | 2005 Dec 21.98     | 53726.48            | 52036.6            |
| 5545  | 2005 Dec 23.21     | 53727.71            | 54203.5            |
| 6237  | 2005 Dec 24.59     | 53729.09            | 51920.8            |
| 6238  | 2005 Dec 25.88     | 53730.38            | 50887.6            |
| 5546  | 2005 Dec 27.23     | 53731.73            | 51939.3            |
| 6230  | 2005 Dec 28.57     | 53733.07            | 52401.0            |
| 6231  | 2005 Dec 29.91     | 53734.41            | 48963.7            |
| 6232  | 2005 Dec 31.22     | 53735.72            | 49139.0            |
| 6233  | 2005 Jan 2.24      | 53737.74            | 103433.2           |
| 6235  | 2005 Jan 4.17      | 53739.67            | 51932.1            |
| 6236  | 2005 Jan 5.48      | 53740.98            | 54729.8            |
| 6239  | 2005 Jan 6.92      | 53742.42            | 52241.6            |
| 6240  | 2005 Jan 8.10      | 53743.60            | 54178.4            |



Table 3. HRC-S Derived X-ray Properties of the 47 Tuc Millisecond Pulsars.

| Name                    | Total <sup>a</sup><br>Counts | Background<br>Counts | Extraction<br>Radius | $\log(L_X)^b$<br>(0.5-2.0 keV) | Harmonics <sup>c</sup><br>( $n$ ) | $Z_n^{2c}$ | Significance <sup>c</sup><br>( $\sigma$ ) | $f_{p,\text{radio}}^{c,d}$ | $f_{p,\text{sine}}^{c,d}$ | $f_p^c$ |
|-------------------------|------------------------------|----------------------|----------------------|--------------------------------|-----------------------------------|------------|---|----------------------------|---------------------------|---------|
| 47 Tuc C                | 173                          | 94.8                 | 1''3                 | 30.12                          | 1                                 | 2.5        | 1.5                                       | <76                        | < 100                     |         |
| 47 Tuc D                | 221                          | 94.8                 | 1''3                 | 30.33                          | 2                                 | 21.7       | 3.9                                       | —                          | —                         | 70 ± 21 |
| 47 Tuc E <sup>g</sup>   | 254                          | 94.8                 | 1''3                 | 30.43                          | 1                                 | 12.5       | 3.3                                       | —                          | —                         | 50 ± 19 |
| 47 Tuc F <sup>e</sup>   | 413                          | 80.7                 | 1''2                 | <30.75                         | 1                                 | 10.1       | 2.9                                       | —                          | —                         | 2 ± 12  |
| 47 Tuc G <sup>f</sup>   | 322                          | 80.7                 | 1''2                 | <30.61                         | 1                                 | 1.0        | 1.0                                       | < 100                      | < 100                     |         |
| 47 Tuc H <sup>g</sup>   | 176                          | 94.8                 | 1''3                 | 30.14                          | 2                                 | 12.7       | 2.8                                       | —                          | —                         | 26 ± 20 |
| 47 Tuc I <sup>f,g</sup> | 322                          | 80.7                 | 1''2                 | <30.61                         | 1                                 | 6.0        | 2.3                                       | <81                        | < 100                     |         |
| 47 Tuc J <sup>g</sup>   | 266                          | 94.8                 | 1''3                 | 30.46                          | 1                                 | 6.5        | 2.3                                       | <38                        | <77                       |         |
| 47 Tuc L                | 342                          | 35.9                 | 0''8                 | 30.71                          | 2                                 | 10.0       | 2.4                                       | <50                        | < 49                      |         |
| 47 Tuc M                | 151                          | 94.8                 | 1''3                 | 29.98                          | 1                                 | 2.2        | 1.4                                       | < 100                      | < 100                     |         |
| 47 Tuc N                | 186                          | 94.8                 | 1''3                 | 30.19                          | 1                                 | 4.8        | 2.0                                       | <73                        | < 100                     |         |
| 47 Tuc O <sup>g</sup>   | 431                          | 94.1 <sup>h</sup>    | 1''2                 | 30.77                          | 3                                 | 39.1       | 5.1                                       | —                          | —                         | 81 ± 21 |
| 47 Tuc Q <sup>g</sup>   | 186                          | 94.8                 | 1''3                 | 30.19                          | 6                                 | 28.3       | 3.1                                       | —                          | —                         | 83 ± 42 |
| 47 Tuc R <sup>g</sup>   | 288                          | 80.4 <sup>h</sup>    | 1''1                 | 30.57                          | 2                                 | 24.1       | 4.1                                       | —                          | —                         | 63 ± 29 |
| 47 Tuc S <sup>e,g</sup> | 413                          | 80.7                 | 1''2                 | <30.75                         | 8                                 | 33.4       | 3.1                                       | —                          | —                         | 20 ± 15 |
| 47 Tuc T <sup>g</sup>   | 133                          | 80.7                 | 1''2                 | 29.94                          | 1                                 | 1.2        | 1.1                                       | < 100                      | < 100                     |         |
| 47 Tuc U <sup>g</sup>   | 193                          | 94.8                 | 1''3                 | 30.22                          | 1                                 | 0.1        | 0.7                                       | < 100                      | < 100                     |         |
| 47 Tuc W <sup>g</sup>   | 433                          | 80.7                 | 1''2                 | 30.77                          | 1                                 | 0.8        | 1.0                                       | <48                        | <48                       |         |
| 47 Tuc Y <sup>g</sup>   | 218                          | 94.8                 | 1''3                 | 30.32                          | 1                                 | 6.5        | 2.3                                       | <40                        | <96                       |         |

<sup>a</sup>This number includes the expect background counts listed in the subsequent column.

<sup>b</sup>X-ray luminosity (logarithm of  $\text{erg s}^{-1}$ ) derived in the band 0.5–2.0 keV.

<sup>c</sup>See the text (§ 3.1) for a description of these parameters.

<sup>d</sup><100% means the undetected pulsation is consistent with 100% pulsed signal, and therefore is unconstrained by simulations.

<sup>e</sup>47 Tuc F and S have overlapping positions. The total counts represent all photons extracted from the 1''2 extraction radius and the background counts are only those expected from a uniform background.

<sup>f</sup>47 Tuc G and I have overlapping positions. The total counts represent all photons extracted from the 1''2 extraction radius and the background counts are only those expected from a uniform background.

<sup>g</sup>Binary MSP.

<sup>h</sup>Includes an estimate of the contamination due to source crowding (see § 3.1).

Table 4. Summary of 47 Tuc MSP Detection Significance.

| Pulsation Detection<br>Threshold<br>(1) | Number of<br>Detections<br>(2) | Binomial<br>Probability<br>(3) | False Detection<br>Probability<br>(4) |
|---|--------------------------------|--------------------------------|---------------------------------------|
| 99%                                     | 8                              | $6.9 \times 10^{-12}$          | 17.5%                                 |
| 99.73%                                  | 6                              | $1.0 \times 10^{-11}$          | 5%                                    |
| 99.947%                                 | 3                              | $1.4 \times 10^{-7}$           | 1%                                    |

Note. — (1) – Confidence level of  $Z_n^2$  above which a 47 Tuc MSP is labeled ‘variable.’ (2) – The number of ‘variable’ MSPs for the given confidence level. (3) – The binomial probability that the number of ‘variable’ MSPs is due to chance. (4) – The probability that one of the ‘variable’ MSPs is a statistical fluctuation.

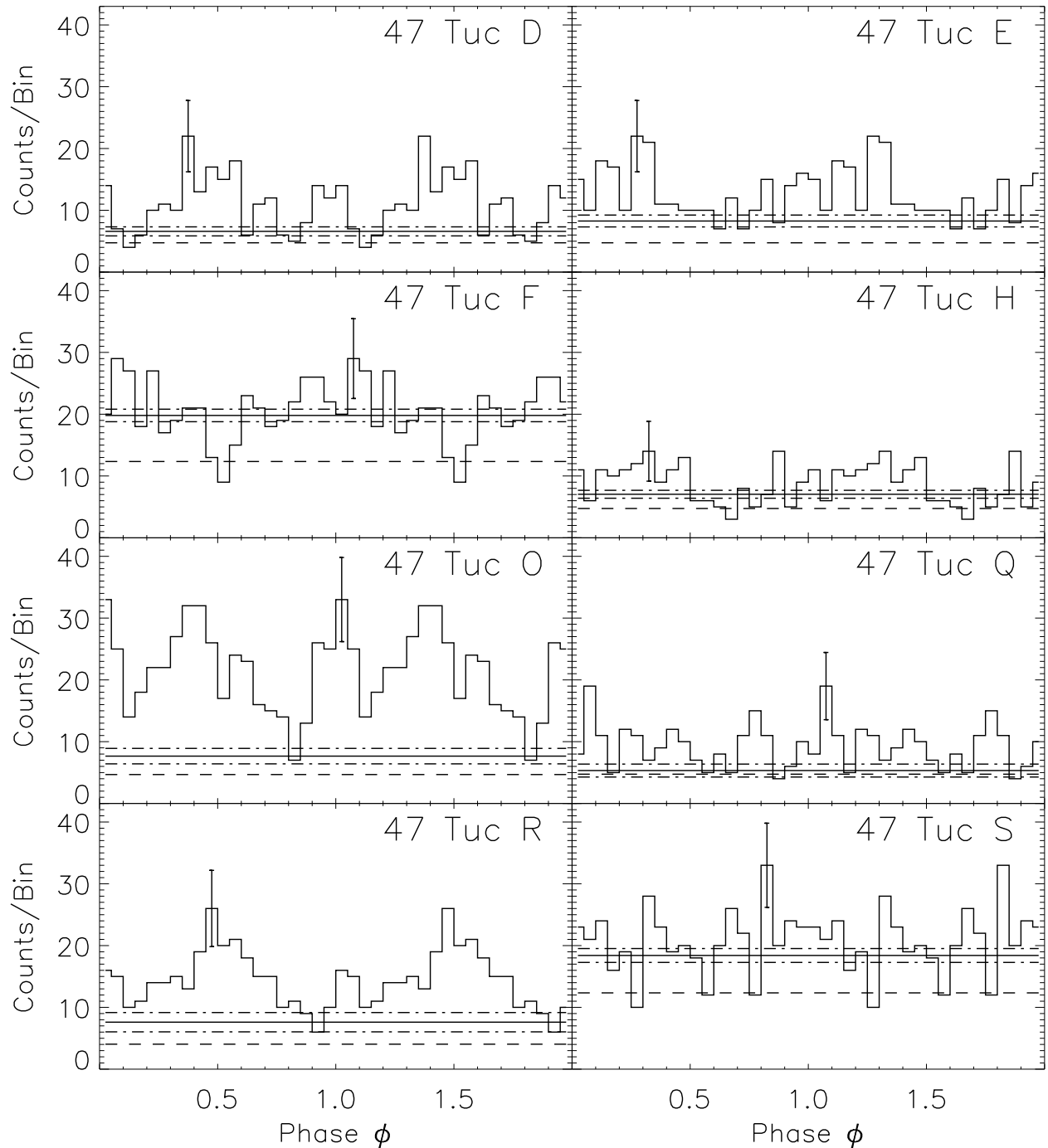


Fig. 1.— Pulse profiles of the variable 47 Tuc MSPs with a typical error bar (two periods are shown for clarity). The histograms were constructed with 20 bins per period. The solid horizontal line denotes the DC (unpulsed) contribution to the pulse profile as determined by the nonparametric bootstrapping algorithm with the associated  $1\text{-}\sigma$  uncertainties denoted with dashed-dotted lines. The dashed line denotes the estimated contribution to this level due to the uniform background and source crowding (50% of the background subtracted counts are attributed to this total for MSPs F and S; see § 3.1 for details).

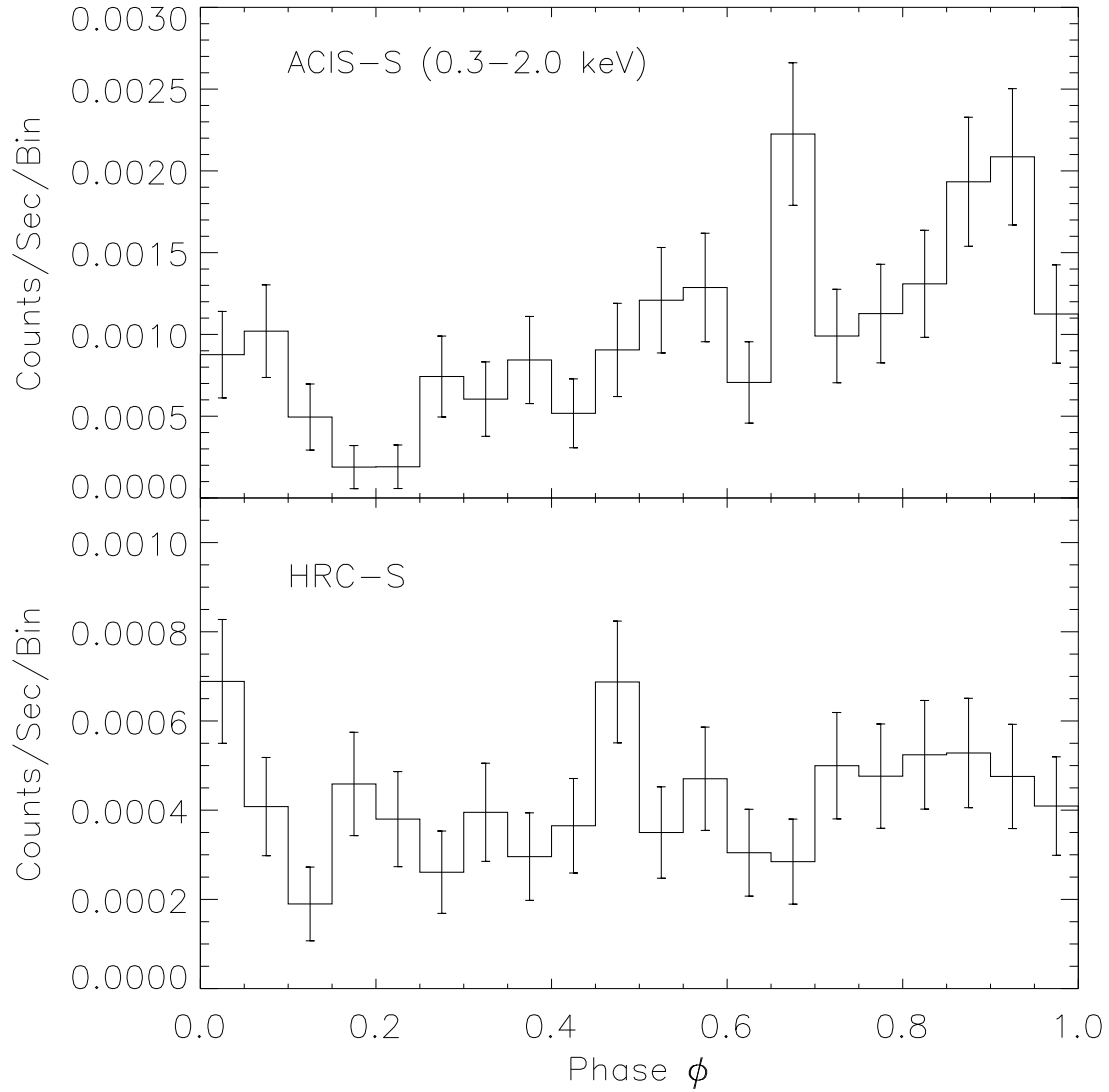


Fig. 2.— Orbital Profiles of 47 Tuc W from ACIS-S (upper) and HRC-S (lower). The error bars are  $1\text{-}\sigma$  and histograms contain 20 bins per period.

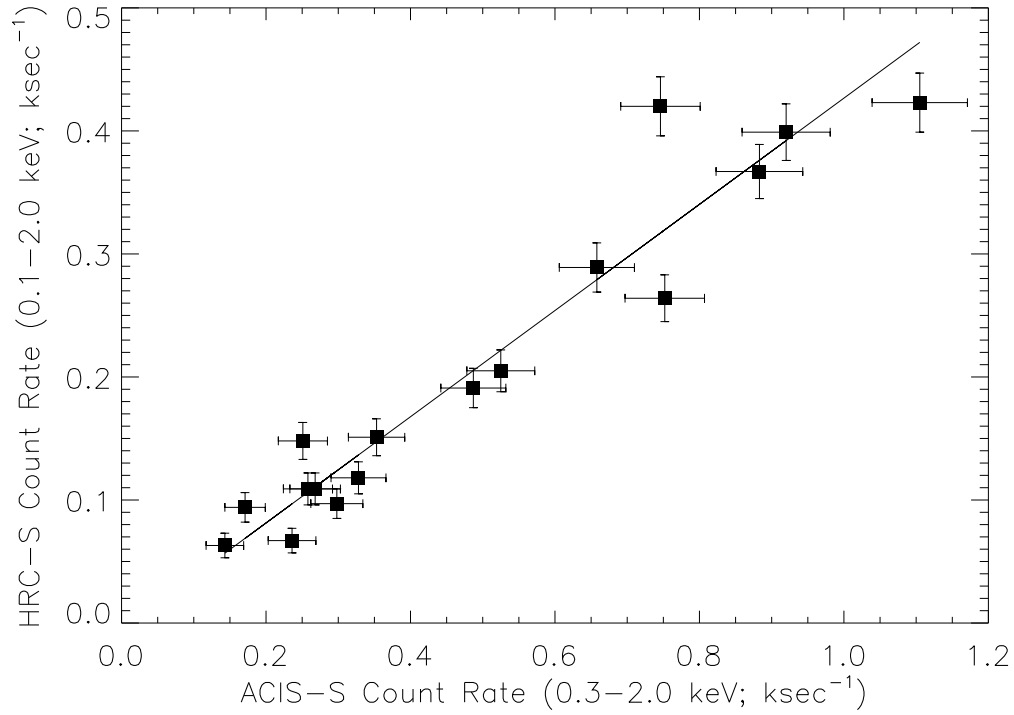


Fig. 3.— HRC-S/ACIS-S count rate comparison using the 17 independent 47 Tuc MSP detections. The line represents the best linear fit to the data.